The lattice stability and structure of delta -UZr_2 at elevated temperatures

1995 J. Phys.: Condens. Matter 7 8249

(http://iopscience.iop.org/0953-8984/7/43/005)

J. Phys.: Condens. Matter 7 (1995) 8249–8257. Printed in the UK

The lattice stability and structure of δ-UZr_2 at elevated temperatures

Mitsuo Akabori, Toru Ogawa, Akinori Itoh and Yukio Morii
Japan Atomic Energy Research Institute, Tokai-mura, Naka-gun, Ibaraki-ken, 319-11 Japan

Received 11 April 1995

Abstract. The lattice stability and structure of δ-UZr_2 were studied by thermal analysis and high-resolution neutron diffraction techniques. The δ structure was confirmed to be the modified C32 (AlB_2-type) structure as in the ω phase of Zr. The temperature dependence of the lattice parameters in the δ phase was determined between room temperature and 880 K. The heat effects at the phase transition from δ to bcc solid solutions were determined to be 5.6–4.4 kJ g-atom^{-1} for $X_{Zr} = 0.67$–0.81. From the composition dependence, the transition enthalpy from ω to β (bcc) phase in pure Zr was estimated to be 2.8 kJ g-atom^{-1}.

1. Introduction

The high-temperature Zr- or Ti-based bcc solid solutions may transform to metastable phases called ω at low temperatures [1]. The ω phase is one of the most extensively studied metastable phases, since its existence in the alloys has various implications for their physical properties. The ω phase is also obtained from the α (hcp) phases of Ti and Zr when high pressures are applied. There is a stable intermediate phase, δ-UZr_2, in the U–Zr binary system [2, 3], as shown in figure 1. The entire U–Zr binary phase diagram plotted in terms of the Zr atomic percentage is shown in figure 1(a). In figure 1(b) [5], part of the U–Zr binary phase diagram is plotted against the U content for ease of comparison with the pressure–temperature (P–T) phase diagram in figure 1(c) [1, 4]. It is difficult to determine the exact homogeneity range of δ-UZr_2, because it exists only at lower temperatures where equilibration takes a very long time. It would also be extremely sensitive to the contents of gaseous impurities—oxygen and nitrogen [5]. Though the assessed phase diagram by Sheldon and Peterson [2] gives the δ homogeneity range as 63–78 at.% Zr, a series of metallographic studies with electron-probe microanalysis showed that it might be a little wider, 63–82 at.% Zr [3].

The structure of δ, which is formed on cooling from the high-temperature bcc solid solutions, (γ-U, β-Zr), has been considered to be closely related to that of ω. The stabilization of the ω structure in Zr at high pressures has been attributed to the increased d-band occupancy at high pressures. That the ω structure is also stabilized by adding U to Zr suggests that there is an appreciable mixing of the U valence shell and Zr d shell, resulting in an increase in the Zr d-band occupancy [5]. Besides the U–Zr system, the $AnZr_2$ (An: actinide) phases with ω-like structures have been found in Np–Zr, Pu–Zr binaries [6, 7].

In a previous study [3], we have reported the homogeneity range and crystal structure of δ-UZr_2. The crystal structure was examined by x-ray diffraction. The x-ray powder

0953-8984/95/438249+09$19.50

diffraction patterns at room temperature agreed well with those based on an unusual modified C32 (AlB_2-type) structure proposed by Boyko [8] and Silcock [9], where the Al positions are preferentially occupied by Zr atoms and the B positions randomly shared by U and Zr atoms. However, there were subtle differences in peak intensities between the observed and calculated patterns. The same kind of disagreement has been reported by Boyko [8]. In this study, the structure of the δ-UZr_2 phase was re-examined by high-resolution neutron diffraction. The lattice stability of δ against the bcc solid solutions was investigated by thermal analysis.

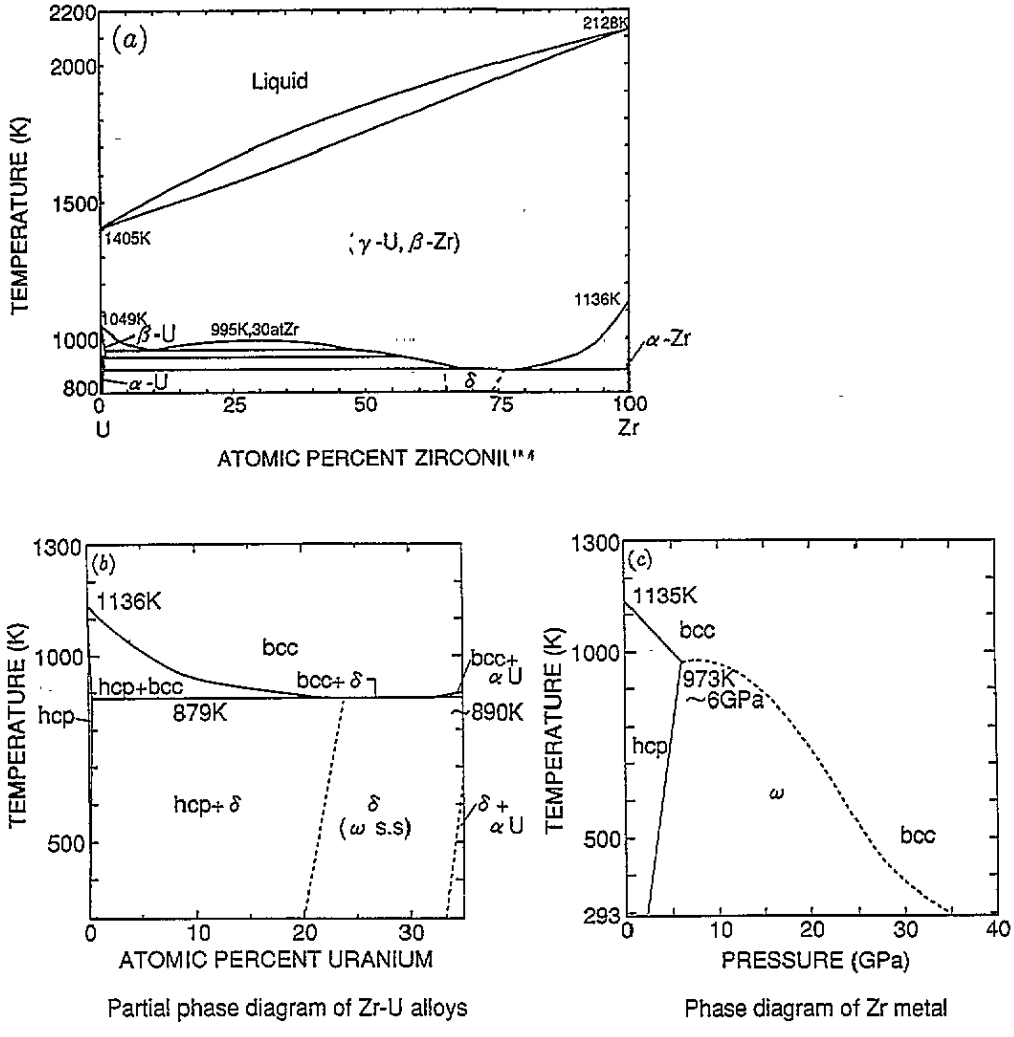

Figure 1. (a) the U–Zr binary phase diagram calculated with the thermodynamic model in [13], (b) a part of the binary phase diagram [5], and (c) the pressure–temperature phase diagram of pure Zr [1, 4]. (b) A plot against the uranium contents for ease of comparison with the P–T diagram in (c). The exact composition range of δ is ambiguous [5] (see text).

2. Experimental details

2.1. Sample preparation

The U–Zr alloys with 11 compositions from 5 to 95 at.% Zr were prepared by arc-melting together high-purity uranium and zirconium metals in purified argon. The zirconium metal was a crystal bar made by iodide refining, which was supplied by the Teledyne Wah Chang Albany; metallic impurities were less than 840 ppm in weight (main impurities : Fe, Hf, Ti and Al). Major metallic impurities in the uranium metal were Al (16 ppm), Fe (16 ppm) and Si (12 ppm) as determined by emission spectrochemical analysis. Oxygen contents in the uranium and zirconium metals were determined by gas chromatography to be 50 and 140 ppm in weight, respectively, while the nitrogen contents were less than 40 ppm in weight. Each alloy button was melted six times to ensure homogeneity. The alloy buttons obtained were wrapped in pure tungsten foils and then sealed in quartz ampoules, which were evacuated at room temperature to 1×10^{-2} Pa and then filled with high-purity helium to 2×10^{4} Pa. All buttons were homogenized at 1123 K for 72 h and then quenched in water. The oxygen and nitrogen contents after the heat treatment were analysed for the U–70.7 at.% Zr alloy and found to be less than 60 and 30 ppm in weight, respectively.

2.2. Neutron diffraction

Neutron diffraction was performed using the HRPD (high-resolution powder diffractometer) at the JAERI research reactor, JRR-3M, which is equipped with a position sensitive detector of 64 cells covering 160 degrees in the 2θ range. The neutron diffraction patterns were measured over the scattering angles from $2\theta = 5°$ to 165° in 0.05° steps, using an incident wavelength of 0.1823 nm from a Ge(331) monochromator. The neutron flux was about 1×10^{5} $cm^{-2}s^{-1}$ at the sample position. The sample consisted of ~1000 small cubes of $1 \times 1 \times 1$ mm^3, which were sliced from a U–70.7 at.% Zr alloy button. The cubes were stacked in a cylindrical aluminium container for room temperature and a vanadium container for high temperatures; the holders had inner dimensions of 7 mm × 50 mm. The containers were filled with high-purity helium to avoid sample oxidation. High temperatures were attained by a standard vacuum furnace, which consisted of two flat-plate resistance heaters. In the room temperature diffraction, the sample was spun about the z-axis of the cylindrical container at about 10 rpm to minimize orientation effects, but in the high-temperature diffractions the sample rotation could not be done. The diffraction patterns were analysed using a Rietveld profile refinement program, RIETAN [10].

2.3. Thermal analysis

The thermal analysis was performed with a high-temperature quantitative DTA/DSC instrument (Sinku-Riko, Inc.). This newly designed unit has an inner platinum furnace and a silicon carbide heating block to make the temperature distribution of the sample zone as uniform as possible. The sensitivity and stability were significantly improved with this arrangement. A platinum sample holder, which was lined inside with Al_2O_3 powder to prevent a reaction between sample and holder, was used. High-purity α-Al_2O_3 powder was used as the reference sample. The alloy samples were cubes of $2 \times 2 \times 1$ mm^3, which were cut from the alloy buttons homogenized at 1123 K. Some cubes were annealed at 823 K, which is slightly below the δ/bcc transition temperatures. Since the cubes themselves were too small for further characterization, some control specimens were heat treated in the same manner and characterized by x-ray diffraction. For highly reactive samples like the

uranium alloys used in this study, extra precautions were required in the thermal analysis. The Ar gas for the sample region of the DTA was passed through two purifier columns containing a molecular sieve and an oxygen getter, to continuously remove water and oxygen contaminations. Before the measurements, the sample part was evacuated and flushed with Ar a few times. The measurements were carried out at a heating rate of 5 K min^{-1} from room temperature to 1123 K.

The temperature and enthalpy, ΔH_t, of transformation were calibrated using two transitions of pure uranium metal, namely, α to β at 941 K with $\Delta H_t = 2.8$ kJ mol^{-1}, and β to γ at 1048 K with $\Delta H_t = 4.8$ kJ mol^{-1} [11]. The enthalpy data were obtained only on the first heating run to minimize the effect of sample oxidation, because adsorbed gas and water in the DTA system could not be completely eliminated. A prolonged heating resulted in sample oxidation, which broadened the temperature range of transition and decreased the transition enthalpy.

3. Results and discussion

3.1. Neutron diffractions

The structural refinements were carried out with the following assumptions; Zr atom occupies the Al position, (0, 0, 0) and a random mixture of U and Zr atoms occupies the B position, (1/3, 2/3, 1/2) and (2/3, 1/3, 1/2), of the C32 (AlB_2-type) hexagonal cell. This structure has been tentatively determined by x-ray diffraction [3]. However, there were noticeable discrepancies in the x-ray peak intensities at 110, 300, 220 and so on, all of which corresponded to the peaks of the high-temperature bcc phase. This is considered to be due to a twinned crystal formed by quenching the bcc solid solutions to the δ phase. The twinned crystal has four hexagonal cells and results in an x-ray pattern resembling that of the bcc structure. One may regard this as a δ phase forming with a large bcc cell having a lattice parameter three times that of the bcc solid solutions. The other factors causing disagreement between the measured and calculated powder pattern would have been surface oxidation and preferred crystal orientation, because the powder was obtained by filing the alloy button and then annealing. In neutron diffraction, the effects of surface oxidation and orientation can be significantly reduced.

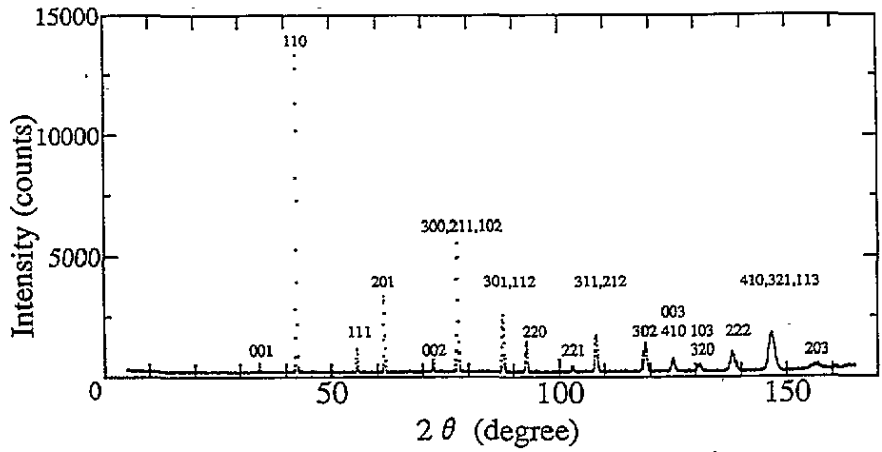

Figure 2. The observed neutron diffraction pattern of U–70.7 at.% Zr alloy.

Table 1. The Rietveld refined parameters obtained for U–70.7 at.% Zr alloys.

Diffraction	Temperature (K)	Phase	Lattice parameter (nm) a	Lattice parameter (nm) c	Isotropic thermal parameter (nm^2) Zr	Isotropic thermal parameter (nm^2) U	Sample R_I (%)	Rotation
X-ray†	Room	δ	0.5028	0.3090	—	—	22.4	X
Neutron	Room	δ	0.50317 ± 0.000 01	0.308 88 ± 0.000 01	0.0031	0.0250	5.19	○
	665	δ	0.5051	0.3095	—	—	—	X
	765	δ	0.5060	0.3096	—	—	—	X
	815	δ	0.5065	0.3097	—	—	—	X
	865	δ	0.5070	0.3097	—	—	—	X
	875	δ	0.5071	0.3097	—	—	—	X
	880	δ	0.5071	0.3097	—	—	—	X
	925	bcc	0.3589	—	—	—	—	X
	975	bcc	0.3592	—	—	—	—	X

† 70.2 at.% Zr.

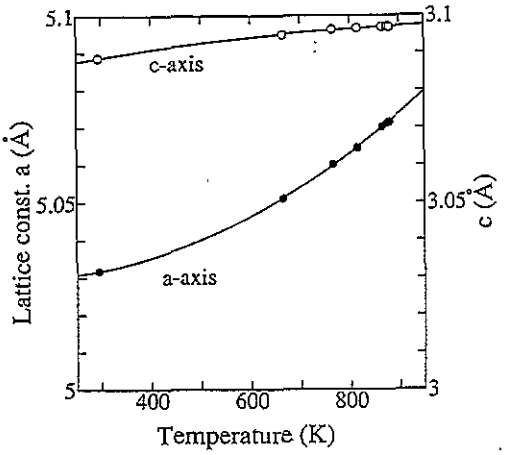

Figure 3. The temperature dependence of the lattice parameters of U–70.7 at.% Zr alloy.

The observed neutron diffraction profile for the 70.7 at.% Zr alloy is shown in figure 2. In the neutron diffraction, the partitioning of U between the Al and B positions has little effect on the diffraction profile, because of a small difference in the atomic scattering factor between U and Zr. Except for this inherent ambiguity, there was a good agreement between the observed and refined profiles. As shown in table 1, the error factor, which is an integrated intensity factor defined by $R_I = \Sigma_j |I_j(o) - I_j(c)| / \Sigma I_j(o)$, was significantly smaller than that obtained by x-ray diffraction. Here, $I_j(o)$ and $I_j(c)$ are the observed and calculated integrated intensities of j reflection, respectively [10]. In the high-temperature diffraction, precise refinement was impossible due to the orientation effect, since the sample could not be rotated in those measurements. The values of R_I for the high-temperature measurements were consequently larger than that obtained at the room temperature. The lattice parameters are relatively insensitive to the structural refinement; figure 3 shows their temperature dependences. The lattice parameters, a_{hex} and c_{hex}, of the hexagonal cell were

fitted:

$$a_{hex}\ (\text{nm}) = 0.5030 - 1.67 \times 10^{-6}T + 7.22 \times 10^{-9}T^2 \quad (1)$$

$$c_{hex}\ (\text{nm}) = 0.3081 + 2.95 \times 10^{-6}T - 1.31 \times 10^{-9}T^2 \quad (2)$$

where T is in kelvin. The lattice parameters of the bcc solid solution at 70.7 at.% Zr were a_{bcc}= 0.3589 and 0.3592 nm at 915 and 965 K, respectively. Generally, the hexagonal cell of the ω phase is oriented with respect to the bcc cell with $\langle 0001\rangle_{hex} \parallel \langle 111\rangle_{bcc}$ and $\langle 2110\rangle_{hex} \parallel \langle 101\rangle_{bcc}$. Ideally, a_{hex} and c_{hex} are related to a_{bcc}:

$$a_{hex} = \sqrt{2}a_{bcc} \quad (3)$$

$$c_{hex} = (\sqrt{3}/2)a_{bcc}. \quad (4)$$

Hence, the ideal c/a ratio for the hexagonal structure is 0.612 ($\sqrt{3/8}$). However, the c/a ratios of the ω phase alloys are usually different from this ideal value [1]. The temperature dependence of the c/a ratio for the δ-UZr_2 phase is shown in figure 4. The c/a ratio decreases gradually with increasing temperature, and becomes less than the ideal ratio above 500 K. The atomic volume as a function of temperature is shown in figure 5. The alloy expands its volume on transition from δ to bcc. The increase in atomic volume was 0.3% at the transition temperature of 885 K, which corresponds to 0.04 $cm^3\ mol^{-1}$. In the case of pure Zr, the volume relationship of $V_\omega < V_{bcc} < V_{hcp}$ has been experimentally estimated from volume changes near the triple point, 6 GPa and 975 K, on the P–T phase diagram [1]: $V_{\omega\rightarrow bcc} \sim 0.1\ cm^3\ mol^{-1}$.

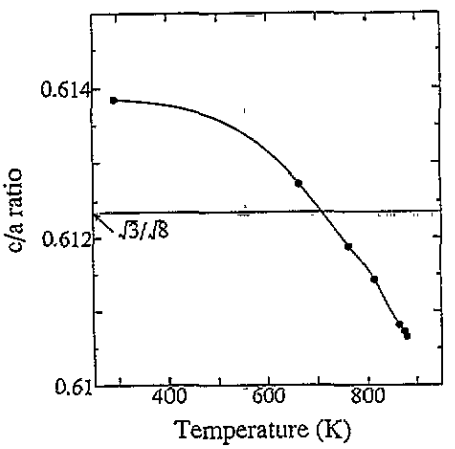

Figure 4. The temperature dependence of c/a values of U–70.7 at.% Zr alloy.

3.2. Thermal analysis

Figure 6 shows typical DTA curves on heating runs for U–12, 70 and 95 at.% Zr alloys, which were homogenized at 1123 K for 72 h. Sharp peaks observed at around 880 K correspond to apparent δ/bcc transitions. The δ phase is actually formed by two reactions [2]: an eutectoid in the U-rich region at ~890 K, α-U + bcc $\rightarrow$ δ, and a peritectoid in the Zr-rich region at 879 K, bcc $\rightarrow$ $\delta + \alpha$-Zr. A two-phase (δ + bcc) region exists for a narrow temperature range (~5 K) at compositions of 63–82 at.% Zr [3]. Thus, a δ-phase alloy in this composition range gradually transforms into a bcc alloy with increasing temperature, giving a somewhat broadened transition peak in DTA. The transition temperature and heat

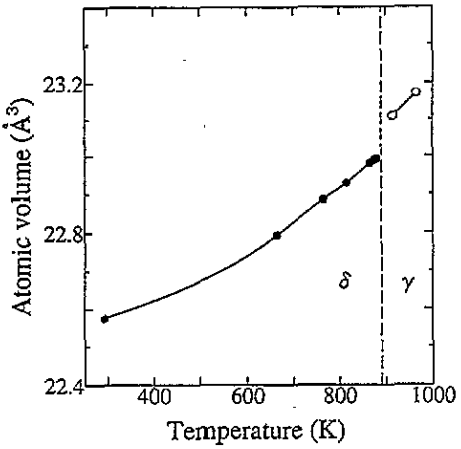

Figure 5. The temperature dependence of the atomic volume of U–70.7 at.% Zr alloy.

effect are summarized in table 2. Figure 7 shows a composition dependence of the heat effect as a function of Zr concentration. There are three regions, α-U + δ, δ and δ + α-Zr, at lower temperatures. The heat effects in the α-U + δ and δ + α-Zr regions appeared proportional to the amount of the δ phase in the sample. The transition enthalpy of a U–20 at.% Zr alloy found by Matsui *et al* [12], 1.57 kJ g-atom^{-1}, is in good agreement with 1.67 kJ g-atom^{-1} at 20 at.% Zr obtained by interpolation in figure 7. The heat effects at the δ/bcc transition for single-phase (δ) alloys depended on the alloy compositions. The heat effects at the δ/bcc transition, ΔH_t, decreased linearly with increasing Zr content from 67 to 81 at.% $\Delta H_t = 10960 - 8130X_{Zr}$ J g-atom^{-1} (5) where X_{Zr} is the atomic fraction of Zr. Corresponding apparent entropy changes, $\Delta H_t/T_t$, are 5–6 J g-atom^{-1} K^{-1}, which are close to $\Delta S_t = 4.8$ J g-atom^{-1} K^{-1} at the ω/bcc phase transition for pure Zr estimated from the P–T phase diagram [1]. With the assumption that δ phase is a series of ω-phase solid solutions, whose validity was confirmed by neutron diffraction, one may extrapolate (5) to $X_{Zr} = 1$ to obtain $\Delta H_t(\omega\text{-Zr} \rightarrow \beta\text{-Zr}) = 2800$ J g-atom^{-1}. This value agrees well with the previous thermodynamic estimation from the phase diagram analysis, which regarded the δ phase as a series of ω-phase solid solutions: $\Delta H_t(\omega\text{-Zr} \rightarrow \beta\text{-Zr}) = 3094$ J g-atom^{-1} [13].

Table 2. The δ/bcc transition characters obtained from the DTA.

Composition (at.% Zr)	Phase	T_t (K)	ΔH_t (kJ g-atom^{-1})	ΔS_t—apparent (J g-atom^{-1} K^{-1})
5.0	α-U + δ	857	0.32	0.37
12.2	α-U + δ	875	0.94	1.07
29.9	α-U + δ	874	2.63	3.01
50.6	α-U + δ	879	3.95	4.49
62.2	α-U + δ	885	5.35	6.05
66.9	δ	882	5.56	6.31
70.5	δ	879	5.17	5.89
80.7	δ	857	4.41	5.15
85.0	δ + α-Zr	867	3.98	4.58
89.7	δ + α-Zr	871	2.51	2.89
95.1	δ + α-Zr	870	1.04	1.20

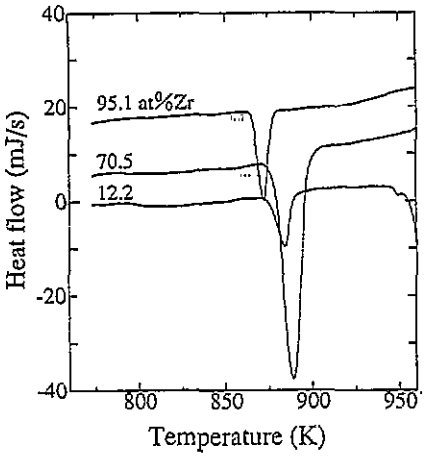

Figure 6. DTA/DSC curves of U–Zr alloys.

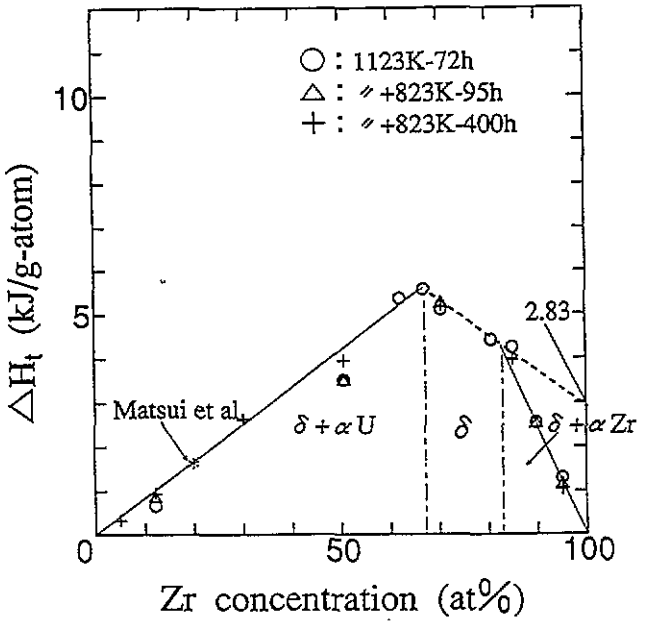

Figure 7. The composition dependence of the heat effects at the δ/bcc transition.

4. Conclusions

The lattice stability and structure of δ-UZr_2 alloys were studied. It was confirmed that the crystal structure is a modified C32 (AlB_2-type) structure via high-resolution neutron diffraction. Therefore, the δ phase may be regarded as a series of ω-phase solid solutions. The atomic volume increased by 0.04 cm^3 mol^{-1} at the δ/bcc transition. Thus, δ has a dense structure like the ω phases with respect to the bcc structure. The heat effects at the δ/bcc transition were determined to be 5.6–4.4 kJ g-atom^{-1} for $X_{Zr} = 0.67$–0.81, and the extrapolation to $X_{Zr} = 1$ suggested that the enthalpy of the ω/bcc transition of pure Zr, $\Delta H_t(\omega\text{-Zr} \rightarrow \beta\text{-Zr})$, is 2800 J g-atom^{-1}.

Acknowledgments

We thank Y Shimojyo for his technical help in measuring the neutron diffraction. We also thank Dr M Handa for his interest and support.

References

[1] Sikka S K, Vohra Y K and Chidambaram R 1982 *Prog. Mater. Sci.* **27** 245
[2] Sheldon R I and Peterson D E 1990 *Binary Alloy Phase Diagrams* vol 3 (Metals Park, OH: American Society of Metals) p 3520
[3] Akabori M, Itoh A, Ogawa T, Kobayashi F and Suzuki Y 1992 *J. Nucl. Mater.* **188** 249
[4] Xia H, Ruoff A L and Vohra Y K 1991 *Phys. Rev.* B **44** 10374
[5] Ogawa T, Gibson J K, Haire R G, Gensini M M and Akabori M 1995 *J. Nucl. Mater.* **223** 67–71
[6] Gibson J K and Haire R G 1992 *J. Nucl. Mater.* **195** 156
[7] Marples J A 1960 *J. Less-Common Met.* **2** 331
[8] Boyko E R 1957 *Acta Crystallogr.* **10** 712
[9] Silcock J M 1957 *J. Met.* **9** 521
[10] Izumi F 1985 *J. Cryst. Soc. Japan* **27** 23
[11] Katz J J, Seaborg G T and Morss L R 1986 *The Chemistry of the Actinide Elements* (London: Chapman and Hall)
[12] Matsui T, Natsume T and Naito K 1989 *J. Nucl. Mater.* **167** 152
[13] Ogawa T and Iwai T 1991 *J. Less-Common Met.* **170** 101